# *Estimating the leaf area index of urban individual trees based on actual path length*

# Estimating the leaf area index of urban individual trees based on actual path length

Hongjie Zhang [a, b], Runming Yao [a, c *], Qing Luo [a, b], Yongchuan Yang [a, d]

[a] Joint International Research Laboratory of Green Buildings and Built Environments, Ministry of Education, Chongqing University, Chongqing, 400045, China

[b] National Centre for International Research of Low-carbon and Green Buildings, Ministry of Science and Technology, Chongqing University, Chongqing, 400045, China

[c] School of the Built Environment, University of Reading, Reading, RG6 6DF, UK

[d] Key Laboratory of the Three Gorges Reservoir Region's Eco-Environment, Ministry of Education, Chongqing University, Chongqing 400045, China

## Abstract

The leaf area index (LAI) is an essential biophysical variable of trees and a crucial factor affecting the urban environment. Previous studies on LAI measurements mainly focused on continuous forests, which using the cosine of the observed zenith angle for path length correction is incompatible with individual trees, although individual trees are more common in urban areas. Therefore, we modified the Beer-Lambert law for individual trees and developed a new path length correction factor that considers crown shape and actual path length in this study. Based on the new path length correction factor, we proposed a systematic single-tree LAI estimation method using digital cover photography. Comparisons with measurements showed that the *root mean square error* (*RMSE*) and *Pearson correlation coefficient* (*r*) are 0.35 and 0.97, respectively. A Python scripted module was compiled to support automated processing of this method. Furthermore, we modeled single-tree crown transmissivity based on the new path length correction factor and provided a simple formula to calculate the transmissivity of the spherical crown using some common assumptions. This study offers a theoretical basis for measuring LAI and calculating the crown transmissivity of individual trees.

**Keywords:** Leaf area index, Individual tree, Crown transmissivity, Digital photography, Beer-Lambert law

**Acronyms**

| | |
|---|---|
| DCP | Digital cover photography |
| DHP | Digital hemispherical photography |
| LAD | Leaf area density |
| LAI | Leaf area index |
| **Nomenclature** | |
| $A$ | The projection area of the tree crown on horizontal ground |
| $G$ | Leaf projection coefficient |
| $h$ | The thickness of the continuous canopy |
| $K$ | The absorption coefficient of the substance |
| $l$ | The path length of the light travels through the substance |
| $l_\theta$ | The actual path length of light through tree crown |
| $l_{ave}$ | The average path length of light through tree crown |
| $LA$ | Half the total leaf area of an individual tree |
| $P$ | Gap fraction |
| $r$ | Pearson correlation coefficient |
| $RMSE$ | Root mean square error |
| $V$ | The crown volume |
| $W_i$ | The weighting factor |
| $\Gamma$ | Gamma function |
| $\eta(\theta)$ | The new path length correction factor for individual trees |
| $\theta$ | View zenith angle |
| $\theta_L$ | Leaf zenith angle |
| $\rho$ | The density of the substance |
| $\tau(\theta)$ | Transmissivity at a view angle of $\theta$ |
| $\Omega$ | The clumping index |

## 1 Introduction

By 2050, about two-thirds of the world's population will live in urban areas [1]. Cities' rapid development has led to various urban environmental problems, including air pollution [2], urban heat islands [3], etc. Tree planting is the most potent way to improve the urban environment by absorption of pollution [4,5], atmospheric cooling [6,7], stormwater mitigation [8,9], and carbon dioxide capture [10]. Improvement effects vary significantly among trees with different biophysical characteristics, such as tree crown size and leaf area index (LAI).

LAI, one-half the total leaf area per unit of the horizontal ground surface, is an essential structural property of trees and a crucial factor affecting the urban environment. Because leaf surfaces are the primary site of energy and mass exchange in processes such as canopy interception and evapotranspiration. Shahidan et al. made a comparison of *Mesua ferrea* L. and *Hura crepitans* L. for solar radiation shielding, and they found that *Mesua ferrea* L., mean LAI is 6.1, reduced radiation by 93%, while *Hura crepitans* L., mean LAI is 1.5, only provided 79% radiation shading [11]. And LAI is also an indispensable input parameter for urban environment simulation software, such as ENVI-met [12]. Three approaches were commonly adopted to acquire LAI, including citing the literature [13,14], selecting from plant databases [15,16], and measuring representative trees [17–19]. Depending on the tree species and growth conditions, LAIs of different tree species differ significantly. This makes it challenging to match LAIs from literature and databases to actual trees. Field measurements seem to be the only way to obtain an accurate LAI.

Field measurements of LAI can be categorized into direct and indirect methods. Direct methods estimate LAI through sampling and area measurement of tree leaves, including destructive sampling [20] and leaf litter collection [21]. When samples are representative, direct methods are considered more accurate than indirect methods. However, direct methods are usually time-consuming and labor-intensive, limiting their applications, so they are only useful for small plants [22].

Indirect methods have become the most commonly used LAI measurement method. Indirect methods are based on the Beer-Lambert law [23], which infers LAI by measuring other variables, such as the leaf projection function and gap fraction [22]. There are three main categories of indirect methods and instruments commonly used: (1) Digital photography, including digital cover photography (DCP) [24,25], and digital hemispherical photography (DHP) [26,27]. (2) Light detection and ranging, including terrestrial laser scanner [28,29], airborne laser scanner [30,31], and spaceborne laser scanner [32,33]. (3) Commercial passive optical instruments, such as LAI-2200 (or the predecessor LAI-2000) Plant Canopy Analyzer [34], SunScan Canopy Analysis System [35], and Tracing Radiation and Architecture of Canopies [36].

The previous study on LAI measurements focused mainly on continuous vegetation, although individual trees are more common in urban areas. However, traditional indirect methods are unreasonable for measuring the LAI of an individual tree because the continuous vegetation assumption is not satisfied. A rigorous review paper stated that "*traditional indirect methods at stand scale should be adjusted for an individual tree, because the cosine of an observation zenith angle for path length correction of a continuous vegetation layer is incompatible for an individual tree*" [22].

Path length correction is crucial for accurately assessing the LAI of an individual tree. However, only two articles related to path length correction were found in the literature databases. The operating manual of the LAI-2200 stipulates that it is necessary to use the actual path length instead of the cosine for path length correction [37]. The LAI-2200, however, is not applicable to LAI measurements of urban individual trees due to radiation blocking in complex urban environments [38]. Hu et al. established a calculation model for laser scanning using the real path length distribution from the reconstructed tree crown envelope and the leaf area density [38]. This algorithm can only be used with terrestrial laser scanners and does not apply to other indirect methods.

Digital photography, with the advantages of permanent image recording and low cost, has gradually become a popular method of measuring LAI due to the development of photography and image processing technology in recent years. This method has been widely used and verified in contiguous vegetation canopy [39–41] and is gradually applied to urban individual trees [18,42–44]. However, these studies directly apply the algorithm of continuous canopies to an individual tree [18,44,45]. Wei et al. assessed three indirect methods for estimating the LAI of individual trees. The results show that digital photography is not recommended for individual trees, and improvements in reliability will depend on new algorithms to account for differences in path length [46]. As a potential method for measuring the LAI of a single tree, a new algorithm that considers path length correction is urgently needed to improve digital photography measurement accuracy.

This study aims to modify the Beer-Lambert law for continuous canopies to apply to individual trees. Define an improved path length correction factor that considers tree crown shape and the actual path length of individual trees. Then establish a systematic LAI measurement method for individual trees using digital cover photography based on the newly-developed path length correction factor. Furthermore, single-tree crown transmissivity is modeled based on the new path length correction factor, and a simple formula for transmissivity with spherical crowns is provided.

## 2 Materials and methods

### 2.1 Modifying Beer-Lambert law for individual trees

#### 2.1.1 Beer-Lambert law for continuous canopies

The law used to describe light attenuation in a homogeneous medium is the Beer-Lambert law [23]. The law states that there is a natural logarithmic relationship between the transmissivity of light through a substance, $\tau$, and the product of the absorption coefficient of the substance, $K$, the density of the substance, $\rho$, and the path length of the light traveling through the substance, $l$:

$$\tau = e^{-k\rho l} \tag{1}$$

When the Beer-Lambert law is applied to a continuous canopy (Fig. 1a), $K$ is substituted by leaf projection coefficient $G$, $\rho$ is substituted by LAD. $h$ is the thickness of the continuous canopy. $1/\cos\theta$ is used to correct the path length of light through the vegetation canopy.

$$\rho = \text{LAD} = \frac{\text{LAI}}{h} \tag{2}$$

$$l = \frac{h}{\cos\theta} \tag{3}$$

Beer-Lambert law underestimates LAI in a non-random distributed canopy, and the clumping index Ω [47] was defined to correct LAI. Ω=1 denotes the random distribution of leaves, $\Omega > 1$ and $\Omega < 1$ represent the regular and clumping distribution, respectively. The classic formula of Beer-Lambert law in a specific zenith angle $\theta$ is established as follows:

$$\tau(\theta) = e^{-\text{LAI}(\theta)\Omega(\theta)G(\theta)/\cos\theta} \tag{4}$$

2.1.2 Beer-Lambert law for individual trees

When the Beer-Lambert law is applied to individual trees (Fig. 1b), the definition of *h* is ambiguous, and the real path length is significantly less than $h/\cos\theta$. In addition, the LAI calculated using Eq. (4) is not comparable at different zenith angles for individual trees because the representative projected area changes while the total leaf area remains constant [38].

The authors provided a new correction factor based on actual path length. $\rho$ is substituted by the LAD of individual trees as same as continuous canopies, and LAD can be calculated as below for individual trees:

$$\text{LAD} = \frac{LA}{V} = \frac{LA\,A}{V\,A} = \frac{\text{LAI}\,A}{V} \tag{5}$$

where $LA$ is half the total leaf area of an individual tree; $V$ denotes the crown volume; $A$ represents the projection area of the tree crown on horizontal ground and can be computed from the maximum tree crown radius. $l$ is substituted by the actual path length, $l_\theta$, of light through the tree canopy. The revised Beer-Lambert law for individual trees is:

$$\tau(\theta) = e^{-\text{LAI}(\theta)\Omega(\theta)G(\theta)/\eta(\theta)} \tag{6}$$

$$\eta(\theta) = \frac{V}{Al_\theta} \tag{7}$$

where $\eta(\theta)$ is the revised path length correction factor for an individual tree. This path length correction factor fully considers the influence of the tree crown shape and actual path length on transmissivity.

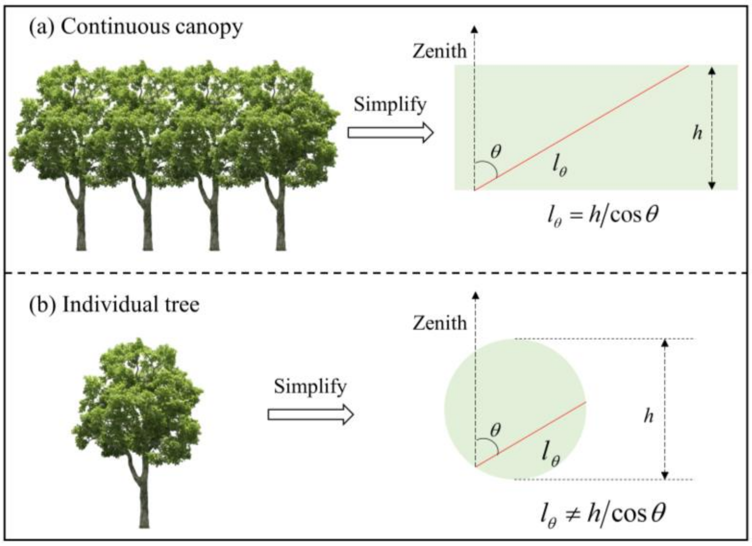


**Fig. 1**. Illustration of the Beer-Lambert law path length for continuous canopies (a) and individual trees (b).

## 2.2 LAI measurement of individual trees using digital photography

In this section, we proposed a digital photography method to measure the LAI of individual trees based on the newly-developed path length correction factor. Digital photography can be classified into digital cover photography (DCP) and digital hemispherical photography (DHP). DCP is used in this paper due to its higher image resolution and insensitivity to camera exposure, gamma correction, canopy density, and mean gap size [39,48]. However, leaf angle distribution needs to be estimated independently to determine LAI using DCP. This study used a mature leveled photography method to parameterize leaf angle distribution [49,50]. The framework for measuring the LAI of individual trees using DCP is shown in Fig. 2.

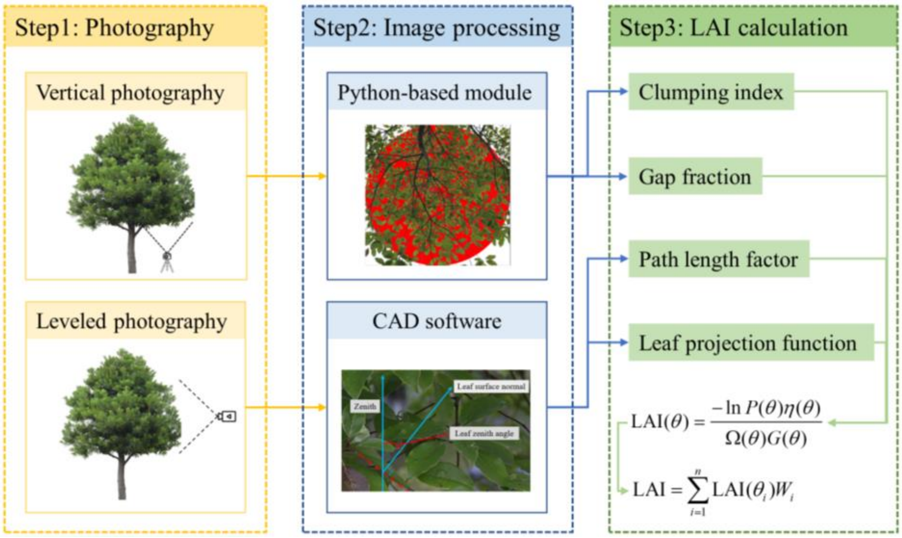


**Fig. 2**. Framework for measuring LAI of individual trees using DCP.

### 2.2.1 Vertical photography

Vertical photography refers to photographing tree crowns from the bottom up. Vertical photography provides images that are used to estimate gap fraction $P(\theta)$ and clumping index $\Omega(\theta)$. Same to continuous canopies, gap fraction $P(\theta)$ is introduced instead of transmission $\tau(\theta)$ to calculate LAI [22]. The camera requires to be fixed with a tripod and placed under the tree crown for vertical photography. The horizontal bubble ensures that the camera is vertically upward. Changing the lens focal length and the camera height ensures that about a quarter of the tree crown is captured while avoiding parts of the sky free of foliage. Taking vertical photography from four directions: front, back, left, and right of the tree crown, as shown in Fig. 3b. These images will be processed using a Python scripted image processing module later.

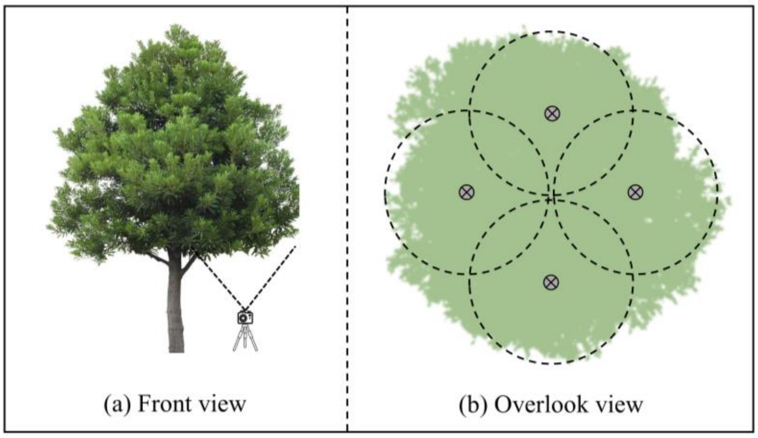

**Fig.3**. Schematic diagram of vertical photography.

2.2.2 Leveled photography

Leveled photography refers to taking pictures in a horizontal orientation. Images taken by leveled photography are used to estimate leaf projection function $G(\theta)$ and path length correction factor $\eta(\theta)$ . Leveled photography is divided into long-distance and short-distance photography based on the distance between the tree crown and the camera. Long-distance leveled photography records the crown shape and the relative position of the vertical camera with the crown, as shown in Fig. 4. To determine the light path length accurately, the long-distance camera should be perpendicular to the plane formed by the tree and the vertical camera, and be at the middle height of the tree crown.

Short-distance photography is a simple and effective method of measuring leaf angles [49,51–53]. Pisek found that reliable estimates of leaf angle distributions at the whole tree level can be obtained by measuring the leaf inclination angles of 75 leaves distributed across the vertical tree profile using digital photography [54]. It is recommended to take photos of the crown from various directions while keeping a short distance between the camera and the crown to ensure accurate identification of leaf angles in the images. These pictures taken in different directions provide statistically significant leaf zenith angles [54].

2.2.3 Image processing and LAI calculation

Long-distance leveled photographic images undergo manual processing using CAD software to measure crown volume, crown projected area, and light path length. The tree crown is vertically layered, and the total crown volume is calculated by adding all layers' volumes together. The crown projected area is calculated from the average crown radius. More specialized programs and methods for estimating crown volume and projected area based on digital photographs have been proposed, especially for irregularly shaped crowns. A detailed introduction to these methods can be found in the review paper by Zhu et al. [55]. The length of the light path passing through the tree crown at different zenith angles is measured based on the relative positions of the vertical photography camera and the crown, as shown in Fig. 4a.

Short-distance leveled photographic images are processed by AutoCAD software to get the zenith angles of leaves with their surfaces oriented approximately perpendicular to the camera's viewing direction (Fig. 4b). The leaf inclination angle distribution of a surveyed tree can be evaluated by assuming a uniform distribution of leaf azimuth angles. The most appropriate and robust Beta-distribution is utilized to present the probability density of $\theta_L$ [56]:

$$f(t) = \frac{1}{B(\mu,\nu)}(1-t)^{\mu-1}t^{\nu-1} \tag{8}$$

where $t = 2\theta_L/\pi$, and $\theta_L$ is expressed in radians. The Beta-distribution is defined as:

$$B(\mu,\nu) = \int_0^1 (1-x)^{\mu-1}x^{\nu-1}dx = \frac{\Gamma(\mu)\Gamma(\nu)}{\Gamma(\mu+\nu)} \tag{9}$$

where $\Gamma$ is the Gamma function, $\mu$ and $\nu$ are calculated as:

$$\mu = (1-\bar{t})(\frac{\sigma_0^2}{\sigma_t^2}-1) \tag{10}$$

$$\nu = \bar{t}(\frac{\sigma_0^2}{\sigma_t^2}-1) \tag{11}$$

where $\sigma_0^2$ is the maximum standard deviation with an expected mean $\bar{t}$, and $\sigma_t^2$ is the variance of $t$. The leaf projection function $G(\theta)$ is calculated as [56]:

$$G(\theta) = \int_0^{\pi/2} A(\theta,\theta_L)f(\theta_L)d\theta_L \tag{12}$$

$$A(\theta,\theta_L) = \begin{cases} \cos\theta\cos\theta_L & |\cot\theta\cot\theta_L| > 1 \\ \cos\theta\cos\theta_L[1+\frac{2}{\pi}(\tan\psi-\psi)] & |\cot\theta\cot\theta_L| \le 1 \end{cases} \tag{13}$$

$$\psi = \cos^{-1}(\cot\theta\cot\theta_L) \tag{14}$$

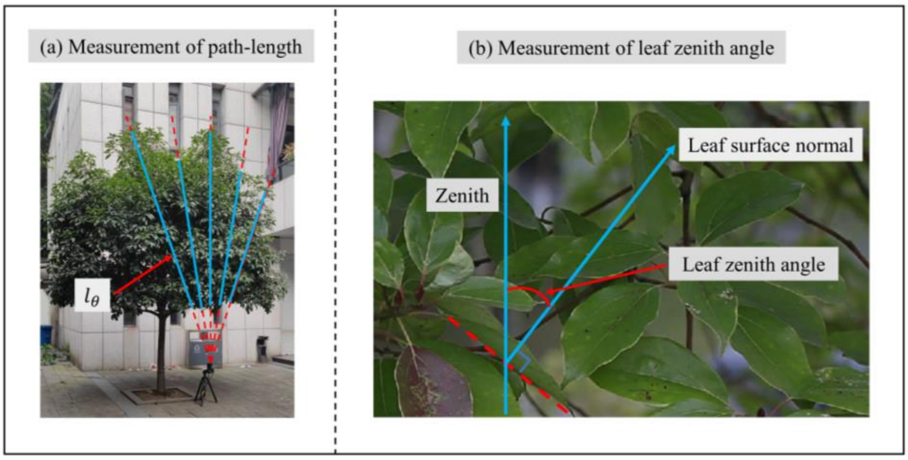


**Fig. 4**. Manual image processing using AutoCAD software.

We compiled a Python script to automate vertical photographic image processing and detailed descriptions can be found in Appendix A. The processing flow of vertical photographic images is shown in Fig. 5. Step 1: Import vertical photographic images. Step 2: Segment the pictures. Divide the images into segments based on the zenith and azimuth angles. Choose ten times the characteristic width of the leaf as the segment length. This is because, theoretically, the error introduced by applying the Beer-Lambert law to this segment length is only about 5 % at this length [22]. Step 3: Identify image elements according to red, green, and blue pixel values (RGB). We preset the default RGB values to be (200, 200, 200), and the values can be manually adjusted to achieve better pixel recognition according to actual photo quality.

$$Outputs = \begin{cases} sky, \;\; if\ color\ RGB \geq (200, 200, 200) \\ tree,\ if\ color\ RGB < (200, 200, 200) \end{cases} \tag{15}$$

When the RGB value is below the preset threshold, the pixel is recognized as a tree element, while those pixels with higher RGB values are sky elements. Finally, the numbers of different elements in each segment (the red pixel in Fig. 5 is the sky element) are counted. The gap fraction $P(\theta)$ is then calculated as the ratio of sky pixels to the total image pixels. The clumping index $\Omega(\theta)$ then can be calculated using the finite-length averaging method [57] as:

$$\Omega(\theta) = \frac{\ln \overline{P(\theta)}}{\overline{\ln P(\theta)}} \tag{16}$$

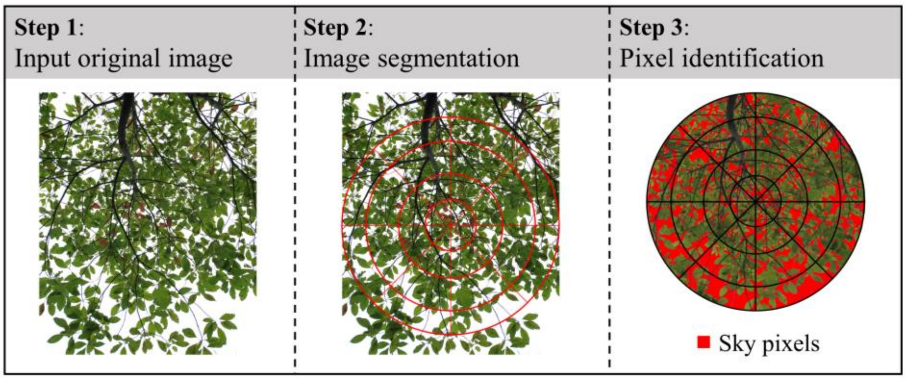


**Fig. 5**. Flow chart for processing vertical photographic images.

Then $\mathrm{LAI}(\theta)$ can be calculated using Eq. (6), and the final LAI can be weighted as follows:

$$\mathrm{LAI} = \sum_{i=1}^{n} \mathrm{LAI}(\theta_i) W_i \tag{17}$$

where $n$ is the number of discrete zenith angles, and $W_i$ is the weighting factor that is proportional to $\sin(\theta_i)d\theta_i$ and normalized to sum to 1.0.

## 3 Methods validation and comparison

In this section, we validated the DCP method based on the newly-developed path length correction factor using the direct method. And then we compared the results with the previous DPC method using the Beer-Lambert law for continuous canopies. The study site is Chongqing University (29° N, 106° E) in Chongqing. Chongqing belongs to the subtropical monsoon humid climate zone, and evergreen trees are the main urban tree species. Five *Osmanthus fragrans* and four *Camphora officinarum* were selected to validate the LAI measurement method based on the revised path length correction factor, as shown in Fig. 6. Two widely used statistical indices were utilized in this study. The *root mean square error* (*RMSE*) uses the square root of the differences between predicted and measured values to represent overall accuracy. The value of *RMSE* is always no less than 0, and a lower *RMSE* means better goodness of fit to the reference value. The *Pearson correlation coefficient* (*r*), between -1 and + 1, measures the linear correlation between predicted and reference values. They are calculated as follows:

$$RMSE = \sqrt{\frac{\sum_{i=1}^{n}(P_i - M_i)^2}{n}} \tag{18}$$

$$r = \frac{\sum_{i=1}^{n}(P_i - \overline{P})(M_i - \overline{M})}{\sqrt{\sum_{i=1}^{n}(P_i - \overline{P})^2}\sqrt{\sum_{i=1}^{n}(M_i - \overline{M})^2}} \tag{19}$$

where $P_i$ is the $i$th predicted value, $M_i$ is the $i$th reference value, $\bar{P}$ is the average of the predicted value, and $\bar{M}$ is the average of the reference value.

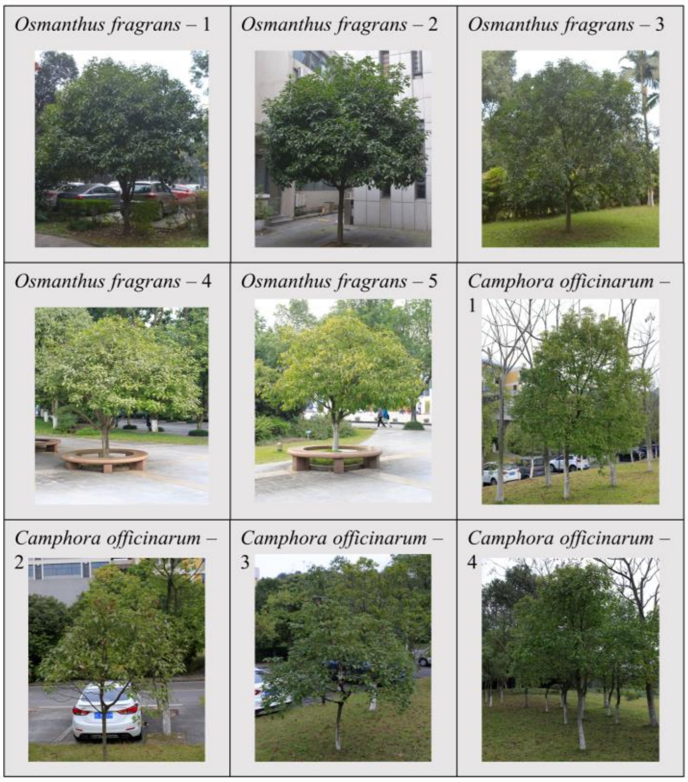


**Fig. 6**. Appearance of nine surveyed trees.

## 3.1 Validation with a direct method

### 3.1.1 Measurement description

Direct methods are often used to validate indirect methods [22]. The LAI values obtained by the standard branch method [58], one of the most commonly utilized direct methods [59], were used as reference LAI values to verify the reliability of the DCP method in this section. The standard branch method includes sampling leaves destructively and measuring the leaf, and the flow chart is shown in Fig. 7. Firstly, we measured the circumference of the branches of surveyed trees (for example main trunk, main branch, end branch, etc.). All branches were divided into five levels based on the branches' circumference, and the number of branches in each level was recorded. Then, select standard branches from the last level and destructively sample from the four directions of east, west, south, and north, and count the number of leaves on the standard branches. Finally, spread the sampled leaves on a whiteboard with a known area, and use the recording and measurement tool of Photoshop software to determine the average area of the sampled leaves. The total leaf area of an individual tree was determined according to the number of last-level branches and the average leaf area. LAI values were then calculated by dividing the total leaf area by the projection area.

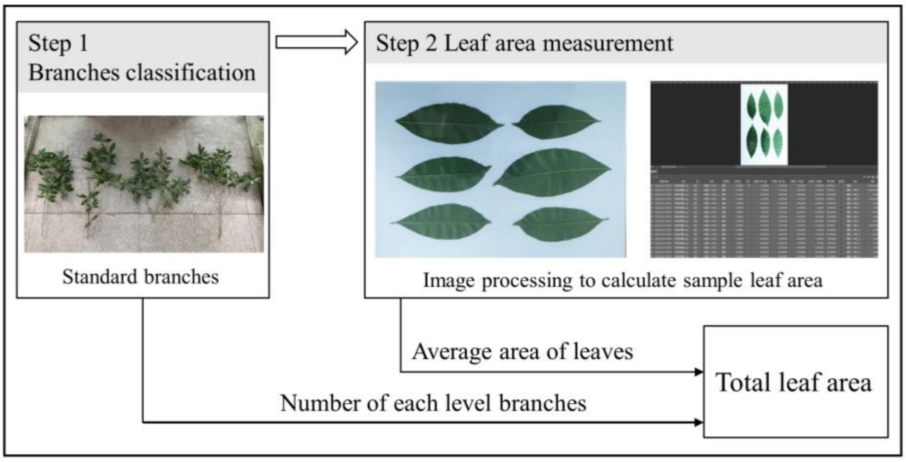


**Fig. 7**. The flow chart of LAI measurements using the standard branch method.

LAI of nine surveyed trees estimated by the standard branch method is shown in Table 1. Tree species play a decisive role in LAI. The average LAI of *Osmanthus fragrans* is generally higher than *Camphora officinarum*, and the mean value is 4.5 and 2.4, respectively. Additionally, the LAI of the same tree species differs significantly. The maximum LAI difference between *Osmanthus fragrans* is 3.7, and the maximum LAI difference between *Camphora officinarum* is 1.3. It is difficult to match the LAI derived from the database and literature research with real trees due to differences in the age, growth status, and density of the canopy of the trees. Therefore, measuring the LAI of the investigated trees in the field is necessary.

**Table 1**
LAI of nine sample trees estimated by standard branch method.

| Sample trees | Leaf area of standard branches ($m^2$) | | | | | Number of standard branches | Projection area ($m^2$) | LAI |
|---|---|---|---|---|---|---|---|---|
| | East | South | West | North | Mean | | | |
| *Osmanthus fragrans* - 1 | 0.440 | 0.411 | 0.388 | 0.358 | 0.399 | 211 | 15.2 | 5.5 |
| *Osmanthus fragrans* - 2 | 0.325 | 0.456 | 0.456 | 0.294 | 0.383 | 199 | 11.3 | 6.7 |
| *Osmanthus fragrans* - 3 | 0.306 | 0.315 | 0.335 | 0.271 | 0.307 | 315 | 23.7 | 4.1 |
| *Osmanthus fragrans* - 4 | 0.287 | 0.305 | 0.265 | 0.253 | 0.278 | 144 | 11.9 | 3.4 |
| *Osmanthus fragrans* - 5 | 0.258 | 0.241 | 0.237 | 0.209 | 0.236 | 128 | 10.2 | 3.0 |
| *Camphora officinarum* - 1 | 0.180 | 0.191 | 0.170 | 0.140 | 0.170 | 127 | 6.9 | 3.1 |
| *Camphora officinarum* - 2 | 0.090 | 0.091 | 0.069 | 0.055 | 0.076 | 74 | 3.1 | 1.8 |
| *Camphora officinarum* - 3 | 0.117 | 0.132 | 0.094 | 0.090 | 0.108 | 45 | 2.2 | 2.2 |
| *Camphora officinarum* - 4 | 0.128 | 0.142 | 0.111 | 0.106 | 0.122 | 98 | 4.8 | 2.5 |

The vertical images were collected using a Canon 5D digital single-lens reflex camera with a 35 mm lens. The aperture was set to F 3.5, automatic exposure, ISO 250, automatic white balance, maximum resolution, and best image quality JPEG. We took photos of each investigated tree from four directions: east, west, south, and north (Fig. 8a). At the same time, we used a mobile phone to take long-distance photography to record the crown shape and the position of the vertical camera. A series of short-distance images of the tree crown were acquired by a camera drone (DJI Mavic 2 Pro) in different directions (front, back, left, and right) and heights (up, middle, and down) of the crown in this study (Fig. 8b).

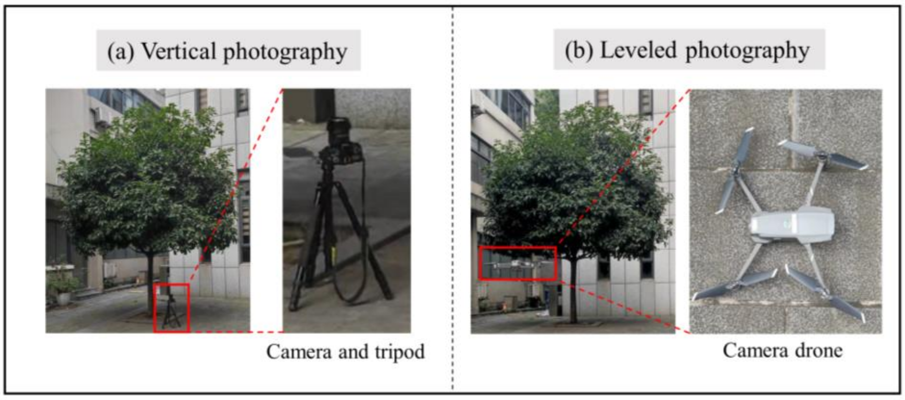


**Fig. 8**. In-situ LAI measurements using the DCP method.

3.1.2 Result validation

The short-distance photographic pictures were imported into CAD software to manually identify the leaves whose surface is approximately perpendicular to the camera's viewing direction and measure the zenith angles. A total of 100 leaf zenith angles were measured from all short-distance photos, a sufficient sample size for estimating leaf inclination distribution [54]. The leaf zenith angles of nine investigated trees were counted, and the results are shown in Fig. 9. Tree species determine the distribution of leaf zenith angles, and there is a similar distribution of leaf zenith angles in trees of the same type. The leaf zenith angle of *Osmanthus fragrans* is mainly concentrated at 15° - 40°, and the number of leaves with a zenith angle exceeding 80° is very small. Among *Camphora officinarum* leaves, the zenith angles are concentrated at 40° - 70°, and small zenith angles ( < 10°) are relatively rare. The red line in Fig. 9 is the probability density of the leaf inclination angle fitted by the Beta-distribution function. Except for *Camphora officinarum* - 3, the sampling values reasonably agree with the Beta-distribution probability density estimates. It may be due to the relatively uniform angular distribution of the leaves of *Camphora officinarum* - 3, and a more accurate Beta-distribution can be obtained by increasing the number of sample leaves. In general, the Beta-distribution is robust for estimating the probability density function of the leaf zenith angle.

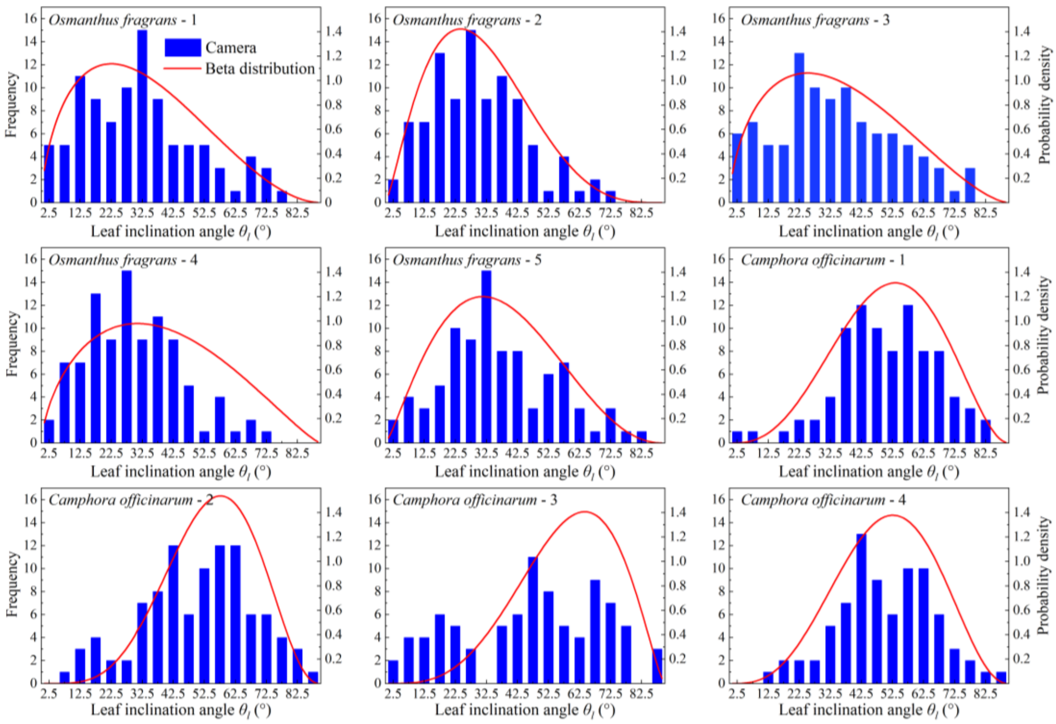


**Fig. 9**. Frequency and Beta-distribution of leaf zenith angle of the studied trees.

According to the probability density of the leaf zenith angle, the leaf projection function of nine surveyed trees was calculated. The leaf projection function of nine trees is shown in Fig. 10. The leaf projection function of five *Osmanthus fragrans* follows an S-shape, and the leaf projection function gradually decreases with the increase of the view angle. The leaf projection functions of the four *Camphora officinarum* do not change much with the increase of the observation angle, and the leaf projection functions are approximately between 0.5 and 0.6. Trees of the same species have similar leaf projection functions for the nine studied trees, but leaf projection functions between different species of trees differ significantly.

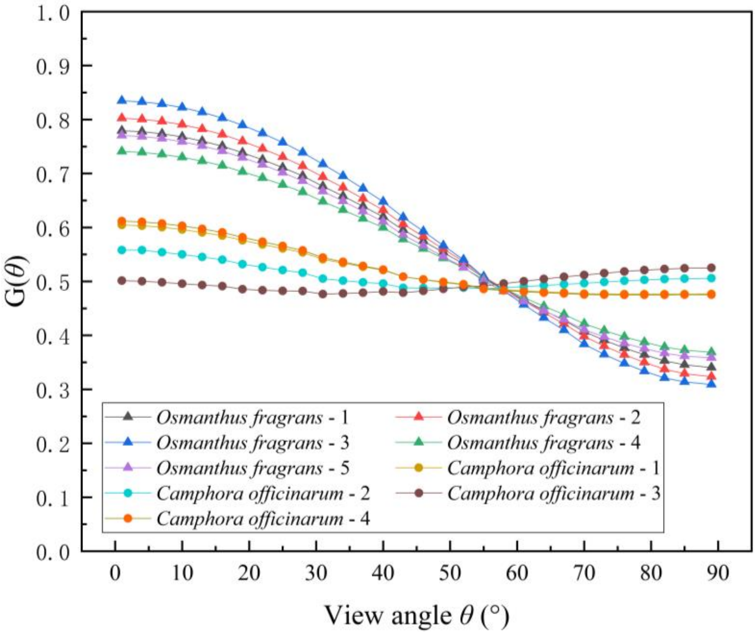


**Fig. 10**. Leaf projection function (*G*) of the nine studied trees.

The images obtained by long-distance leveled photography were imported into AutoCAD. The crown volume, projection area, and light path length were manually measured. The path length correction factor was calculated using Eq. (7). The vertical photographic pictures were imported into the Python scripted module for image processing. The input parameters of the module are shown in Table 2. The images were initially divided into three circular rings (25° - 15°, 15° - 5°, 5° - 0°) based on the zenith angle. Then the circular rings were divided into small segments with an azimuth range of 45°. Pixels with an RGB value greater than 200 are identified as sky elements.

**Table 2**

The input parameters of the image processing module.

| Input parameters | Values |
|---|---|
| Image view angle | 25° |
| Zenith circle range | 10° |
| Azimuth range | 45° |
| RGB threshold | 200 |

All vertical photographic images from the east, west, north, and south were processed. The average LAI values of those four directions were used as the final LAI of the investigated trees. There are quite a few differences between the LAI values obtained from different orientation tests, as shown in Table 3. The LAI of the southward crown is generally larger than that of the northward crown due to the dense foliage and prolonged sun exposure associated with it. Therefore, taking pictures from different directions of the crown and calculating the average LAI values is an effective way to ensure results accuracy. For the nine trees studied, the LAI values measured by the DCP method were compared with direct methods. The LAI values obtained by DCP are in reasonable agreement with the direct method test results ($r$ = 0.97, $RMSE$ = 0.35). The comparison indicates that the DCP method based on the new path length correction factor is effective for measuring individual tree LAI.

**Table 3**

Leaf area index of nine sample trees estimated by DCP.

| Sample trees | Leaf area index | | | | | |
|---|---|---|---|---|---|---|
| | Values estimated by DCP | | | | | Values estimated by the standard branch method |
| | East | South | West | North | Mean | |
| *Osmanthus fragrans* - 1 | 5.78 | 5.38 | 4.61 | 4.33 | 5.0 | 5.5 |
| *Osmanthus fragrans* - 2 | 6.66 | 6.88 | 6.22 | 6.09 | 6.5 | 6.7 |
| *Osmanthus fragrans* - 3 | 3.54 | 4.08 | 3.60 | 3.48 | 3.7 | 4.1 |
| *Osmanthus fragrans* - 4 | 2.80 | 4.42 | 3.98 | 3.22 | 3.6 | 3.4 |
| *Osmanthus fragrans* - 5 | 2.56 | 3.03 | 3.28 | 2.46 | 2.8 | 3.0 |
| *Camphora officinarum* - 1 | 3.92 | 4.27 | 3.13 | 3.53 | 3.7 | 3.1 |
| *Camphora officinarum* - 2 | 1.62 | 2.00 | 2.15 | 2.15 | 2.0 | 1.8 |
| *Camphora officinarum* - 3 | 2.51 | 3.09 | 2.41 | 2.02 | 2.5 | 2.2 |
| *Camphora officinarum* - 4 | 3.11 | 3.14 | 2.37 | 2.72 | 2.8 | 2.5 |

3.2 Comparison with the traditional method for continuous canopies

In this section, we compared the results based on the revised path length correction factor with the previous DPC method using Beer-Lambert law for continuous canopies. We calculated the LAI of the nine individual trees investigated in section 3.1 using formula (4). $\cos\theta$ was used instead of the actual path length correction factor $\eta(\theta)$, and other input parameters remained the same. Fig. 11 shows the comparison results. For the nine trees surveyed, the maximum relative error was 19.4% when the actual path lengths were considered (represented by filled squares), which increased to 36.4%

when the traditional path length correction factor was applied (represented by empty squares), and the $r$ decreased from 0.979 to 0.914. The results show that an algorithm based on the actual path length is necessary for evaluating the LAI of individual trees.

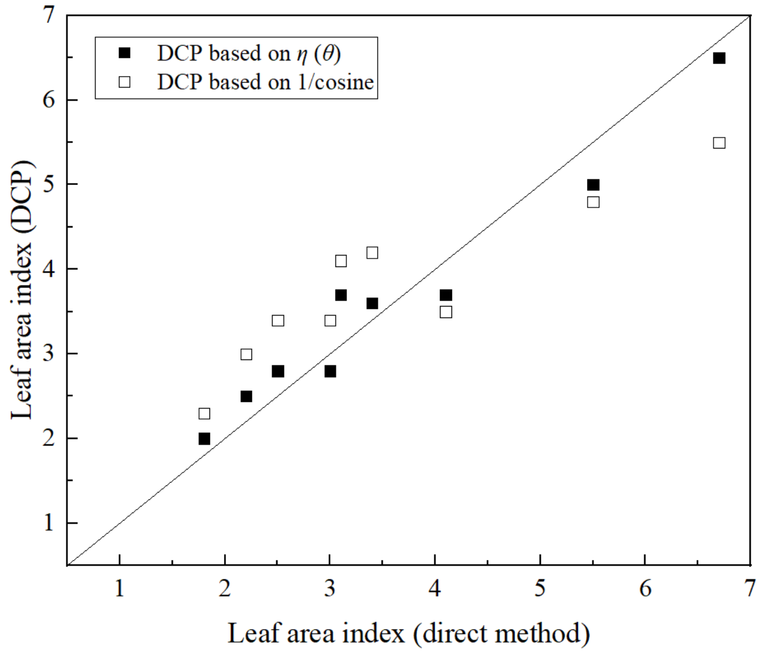


**Fig. 11**. Comparison with the traditional path length correction factor for continuous canopies.

## 4 Discussion

### 4.1 Path length correction factor of typical crown shapes

The new path length correction factor considers the impact of tree crown shape and actual light path length on LAI. Theoretically, $\eta(\theta)$ can also be applied to continuous vegetation canopies. Suppose the radius of the continuous vegetation canopy is $r$, and the canopy thickness is $h$. The vegetation canopy volume is $h\pi r^2$ and the crown projected area is $\pi r^2$. $\eta(\theta)$ can be simplified to $\cos\theta$ for continuous vegetation canopy. That is, $\eta(\theta)$ and $\cos\theta$ are consistent for continuous vegetation canopies, which verifies the rationality and effectiveness of the new path correction factor from a theoretical perspective. Due to manual pruning, urban trees have a more regular crown shape. For the convenience of calculation, we calculated the $\eta(\theta)$ for typical crown shapes, as shown in Table 4.

**Table 4**

The path length correction factor of typical tree crown shapes.

| Crown shapes | Canopy volume | Crown projected area | $\eta(\theta)$ |
|---|---|---|---|
| Sphere | $4\pi r^3/3$ | $\pi r^2$ | $4r/3l_\theta$ |
| Hemisphere | $2\pi r^3/3$ | $\pi r^2$ | $2r/3l_\theta$ |
| Ellipsoid | $4\pi abc/3$ | $\pi ab$ | $4c/3l_\theta$ |
| Cylinder | $h\pi r^2$ | $\pi r^2$ | $h/l_\theta$ |
| Cone | $h\pi r^2/3$ | $\pi r^2$ | $h/3l_\theta$ |

### 4.2 Rapid transmissivity calculation of spherical crown shapes

In this section, we studied the crown transmissivity of individual trees based on the actual path length correction factor. The transmissivity of individual trees was modeled using the following assumptions.

(1) Spherical crown shape

The spherical crown is one of the most popular forms of individual trees. In many models, tree crowns are simplified to spherical (3 D) and circular (2 D) shapes [60–62]. For a spherical crown, the path length of parallel light passing through the crown at any incident angle is constant.

(2) Leaves are approximately randomly distributed within the crown

For a single tree, an approximately random distribution is one of the commonly used spatial distribution assumptions for leaves within crowns [63–65]. Based on this assumption, the clumping index is determined to be a constant ($\Omega = 1$).

(3) Spherical leaf angle distribution

Spherical leaf angle distribution is the basic mathematical description of the angular orientation of leaves in vegetation [22], where leaf normals are oriented in all directions with equal probability ($G = 0.5$).

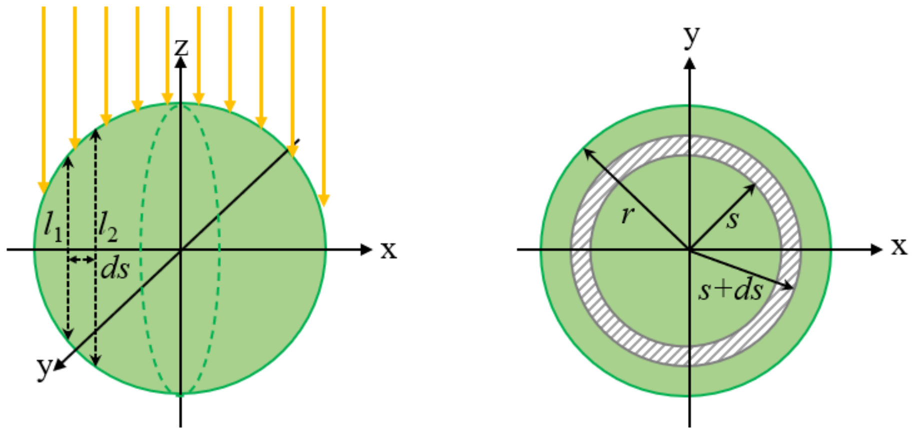


**Fig. 12**. Schematic diagram of parallel light passing through a spherical tree crown.

Based on the above assumptions, when the light is parallel to the *z*-axis, as shown in Fig. 12, the crown transmissivity can be calculated by

$$\bar{\tau} = \int_0^{2r} e^{-LAI \cdot \Omega \cdot G \cdot \frac{Al}{V}} f(l) dl \tag{20}$$

where, $\Omega$, $G$, $A$ and $V$ are constants and shown in Table. 5. According to reference [66], $f(l)$ is

$$f(l) = \frac{l}{2r^2} \tag{21}$$

then the spherical crowns' transmissivity is

$$\bar{\tau} = \int_0^{2r} e^{-LAI \cdot \frac{3l}{8r}} \cdot \frac{l}{2r^2} dl = \frac{32}{9LAI^2}(1 - e^{-\frac{3}{4}LAI}) - \frac{8}{3LAI} e^{-\frac{3}{4}LAI} \tag{22}$$

The relationship between spherical crowns' transmissivity and the LAI of individual trees is shown in Fig. 13. The transmissivity decreases gradually with the LAI increases, the transmissivity is close to 1.0 when the LAI tends to 0.0, and the transmissivity is less than 0.1 when the LAI is larger than 5.7.

**Table 5**

The input parameters of spherical crown transmissivity calculation.

| Symbols | $V$ | $A$ | $\Omega$ | $G$ |
|---|---|---|---|---|
| Values | $4\pi r^3/3$ | $\pi r^2$ | 1 | 0.5 |

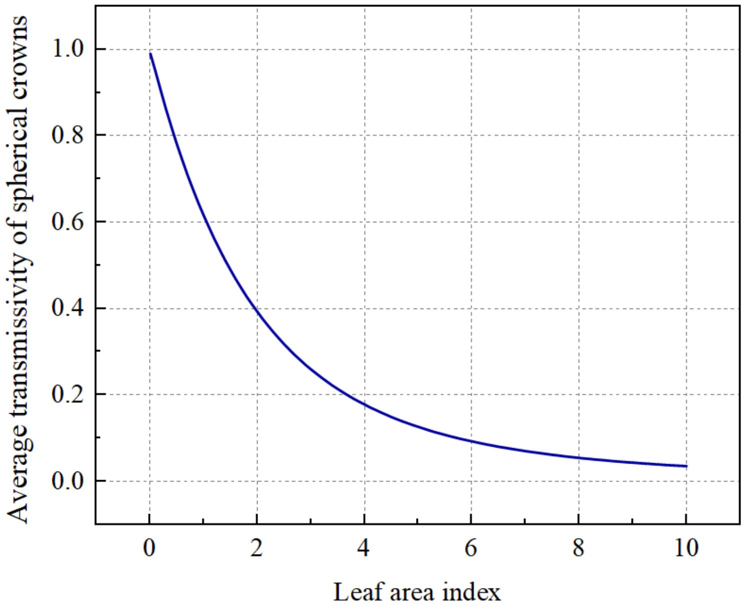


**Fig. 13**. The relationship between spherical crowns' transmissivity and LAI.

### 4.3 Limitations and future works

There are several limitations to this study. First, there is still no field protocol to standardize digital photography methods. All processes are human-operated and errors may occur at any stage of photography and image analysis. It is crucial to comprehensively analyze the sources of errors in digital photography methods and formulate comprehensive test specifications, although this work is very tedious. Second, complex and compact urban structures may make photography difficult. For example, it is not easy to make long-distance photography of trees close to buildings. Finally, although we have developed a module for image processing, this module is simple and can only be used to process vertical photography images. A full-featured software is helpful for automation.

## 5 Conclusions

This study develops a new path length correction factor that considers crown shape and actual light path length. The newly-developed path length correction factor makes Beer-Lambert law applicable to individual trees. The main conclusions are as follows.

(1) A systematic digital cover photography (DCP) method for leaf area index (LAI) estimation of individual trees is proposed based on the new path length

correction factor. Compared with experimental data by direct method, the DCP method proposed in this study performs well. The *root mean square error* (*RMSE*), and *Pearson correlation coefficient* ($r$) are 0.35 and 0.97, respectively. Furthermore, a Python scripted module is developed to serve rapid LAI estimation.

(2) The crown transmissivity of individual trees is modeled based on the new path length correction factor. A simple formula for calculating the transmissivity of spherical tree crowns with some common assumptions is established.

We believe that the newly-developed path length correction factor can offer a theoretical basis for the calculation related to individual tree radiation, and the DPC method and transmissivity calculation formula can contribute to green urban design.

## Acknowledgements

The research is supported by the National Natural Science Foundation of China (Grant No. 52278090), the Ministry of Science and Technology of the People's Republic of China (Grant No. 2022YFC3801504), the Natural Science Foundation funded by Chongqing Government (Grant No. CQYC20200101120).

## Appendix A. Module manual of LAIProcess

We have compiled a Python script module, named LAIProcess, for automated image processing and calculation. This module is based on OpenCV-Python == 4.5.3.56, NumPy == 1.21.0, Pandas == 1.3.2. Please make sure the above modules are installed.

### A.1 Module input parameters

Table A1 lists module input parameters and all input parameters are specified below.

**Table A1**

The input parameters of the LAIProcess module.

| Symbol | Description |
| --- | --- |
| img_src_ori | The storage path of the image to be processed |
| camera_view_angle_ori | The zenith angle of the processed image, which is determined |

| | |
|---|---|
| | by the frame and lens of the camera |
| angle_blank | Zenith circle range |
| line_count | The parameter used to determine the zenith angle range |
| threshold | The pixel threshold used to determine the sky element |
| F($\theta$) | The path length correction factor |
| src | The zenith angle of leaves |

(1) img_src_ori

The storage path of the images. We recommend storing the images to be processed in the static folder. This is the space used by this module to store image data. In addition, commonly used image storage formats are allowed.

(2) camera_view_angle_ori

An accurate zenith angle range of the processed image is necessary. Lens specifications and camera properties determine the zenith angle range of the picture. Fig. A1 shows the relationship between the focal length and viewing angle range. For full-frame cameras, the field of view of the image can be determined directly using the lens focal length according to Fig. A1. However, for half-frame cameras, the focal length must be multiplied by 1.6 with the lens calibration focal length.

When the camera viewing angle is obtained, a second step is required to calculate the zenith angle range of the processed image. The following formula determines the zenith angle range of the processed image:

$$\text{camera\_view\_angle\_ori} = \frac{viewing\_angle \times image\_width}{image\_diagonal\_length} \quad \text{(A1)}$$

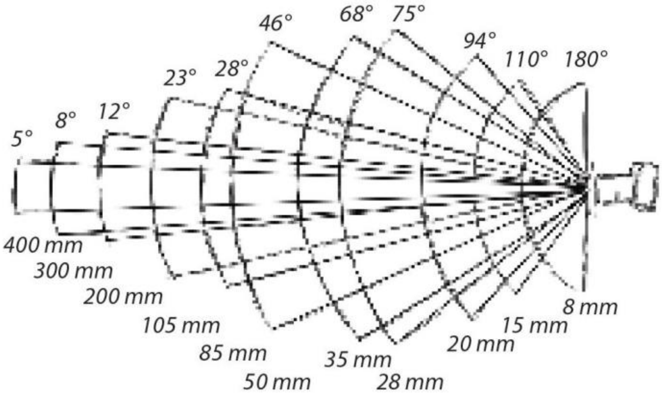

**Fig.A1**. The relationship between the focal length and the viewing angle range.

(3) angle_blank

This parameter determines the zenith range for image segmentation. For example, when angle_blank is equal to 10°, and camera_view_angle_ori is equal to 30°, the image will be divided into three semi-circular rings (30°- 20°, 20°- 10°, 10°- 0°).

(4) line_count

This parameter determines the azimuth range for image segmentation. For example, when line_count equals 1, the azimuth range of small segments is 180°.

(5) threshold

This parameter determines the sky element in the image. For example, when the threshold equals 200, pixels with RGB values greater than 200 are considered sky elements. This parameter can be manually modified by visually inspecting the sky element in the image.

(6) F($\theta$)

The new path length correction factor proposed in this paper is determined by Eq. (7). Where $\theta$ is the average value of the zenith angle of the analyzed fragment.

(7) src

The zenith angle of leaves with their surfaces orienting approximately perpendicular to the camera's viewing direction. The number of measured leaves should be above 75 to ensure statistical significance. Each data is separated by a space in this input parameter.

A.2 Module output

The module will output a series of LAI($\theta$). Users need to calculate the LAI using Eq. (17). Usually, each image can only represent the local canopy, so it is necessary to process photos taken at different locations multiple times to obtain the average LAI of a single tree.

A.3 Module processing

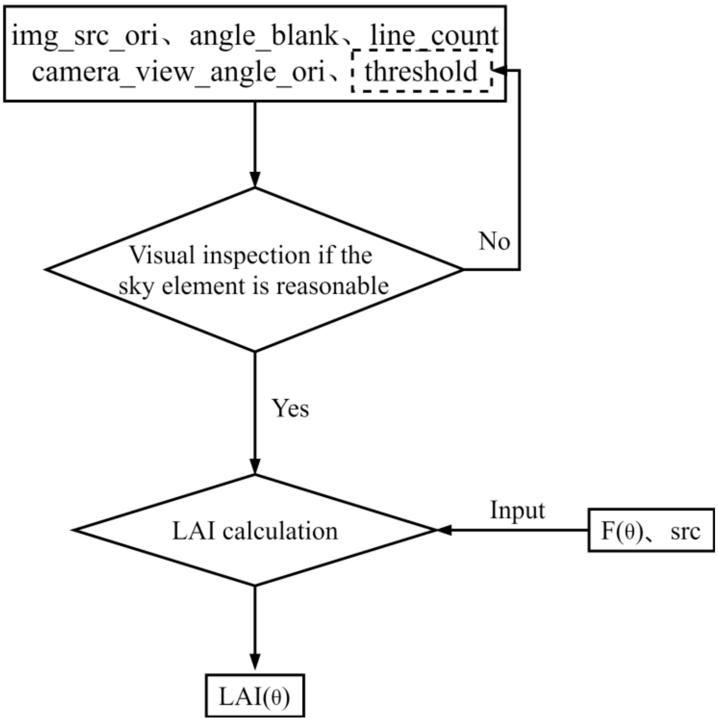


**Fig.A2**. Schematic diagram of the operation of the module.

A.4 Module link

The module has been uploaded to GitHub: LAIProcess.

## References


[1] N. United, World Urbanization Prospects: The 2018 Revision, Online Edition. (2018).

[2] A.J. Cohen, H.R. Anderson, B. Ostro, K.D. Pandey, M. Krzyzanowski, N. Künzli, K. Gutschmidt, C.A. Pope III, I. Romieu, J.M. Samet, Urban air pollution, Comparative Quantification of Health Risks: Global and Regional Burden of Disease Attributable to Selected Major Risk Factors. 2 (2004) 1353–1433.

[3] H.H. Kim, Urban heat island, International Journal of Remote Sensing. 13 (1992) 2319–2336.

[4] C. Letter, G. Jäger, Simulating the potential of trees to reduce particulate matter pollution in urban areas throughout the year, Environment, Development and Sustainability. 22 (2020) 4311–4321.

[5] M. Tallis, G. Taylor, D. Sinnett, P. Freer-Smith, Estimating the removal of atmospheric particulate pollution by the urban tree canopy of London, under current and future environments, Landscape and Urban Planning. 103 (2011) 129–138. https://doi.org/10.1016/j.landurbplan.2011.07.003.

[6] S.K. Gupta, J. Ram, H. Singh, Comparative study of transpiration in cooling effect of tree species in the atmosphere, Journal of Geoscience and Environment Protection. 6 (2018) 151–166.

[7] J.A. Lachapelle, E. Scott Krayenhoff, A. Middel, P. Coseo, J. Warland, Maximizing the

pedestrian radiative cooling benefit per street tree, Landscape and Urban Planning. 230 (2023) 104608. https://doi.org/10.1016/j.landurbplan.2022.104608.

[8] D.E. Carlyle-Moses, S. Livesley, M.D. Baptista, J. Thom, C. Szota, Urban trees as green infrastructure for stormwater mitigation and use, Forest-Water Interactions. (2020) 397–432.

[9] V. Grey, S.J. Livesley, T.D. Fletcher, C. Szota, Establishing street trees in stormwater control measures can double tree growth when extended waterlogging is avoided, Landscape and Urban Planning. 178 (2018) 122–129. https://doi.org/10.1016/j.landurbplan.2018.06.002.

[10] G. Santori, C. Charalambous, M.-C. Ferrari, S. Brandani, Adsorption artificial tree for atmospheric carbon dioxide capture, purification and compression, Energy. 162 (2018) 1158–1168.

[11] Mohd.F. Shahidan, M.K.M. Shariff, P. Jones, E. Salleh, A.M. Abdullah, A comparison of Mesua ferrea L. and Hura crepitans L. for shade creation and radiation modification in improving thermal comfort, Landscape and Urban Planning. 97 (2010) 168–181. https://doi.org/10.1016/j.landurbplan.2010.05.008.

[12] Z. Liu, W. Cheng, C.Y. Jim, T.E. Morakinyo, Y. Shi, E. Ng, Heat mitigation benefits of urban green and blue infrastructures: A systematic review of modeling techniques, validation and scenario simulation in ENVI-met V4, Building and Environment. 200 (2021) 107939. https://doi.org/10.1016/j.buildenv.2021.107939.

[13] S. Tsoka, T. Leduc, A. Rodler, Assessing the effects of urban street trees on building cooling energy needs: The role of foliage density and planting pattern, Sustainable Cities and Society. 65 (2021) 102633. https://doi.org/10.1016/j.scs.2020.102633.

[14] A. Aboelata, Vegetation in different street orientations of aspect ratio (H/W 1:1) to mitigate UHI and reduce buildings' energy in arid climate, Building and Environment. 172 (2020) 106712. https://doi.org/10.1016/j.buildenv.2020.106712.

[15] S. Atwa, M.G. Ibrahim, R. Murata, Evaluation of plantation design methodology to improve the human thermal comfort in hot-arid climatic responsive open spaces, Sustainable Cities and Society. 59 (2020) 102198. https://doi.org/10.1016/j.scs.2020.102198.

[16] D. Antoniadis, N. Katsoulas, C. Kittas, Simulation of schoolyard's microclimate and human thermal comfort under Mediterranean climate conditions: effects of trees and green structures, Int J Biometeorol. 62 (2018) 2025–2036. https://doi.org/10.1007/s00484-018-1612-5.

[17] E. Gatto, R. Buccolieri, E. Aarrevaara, F. Ippolito, R. Emmanuel, L. Perronace, J.L. Santiago, Impact of Urban Vegetation on Outdoor Thermal Comfort: Comparison between a Mediterranean City (Lecce, Italy) and a Northern European City (Lahti, Finland), Forests. 11 (2020) 228. https://doi.org/10.3390/f11020228.

[18] T.E. Morakinyo, L. Kong, K.K.-L. Lau, C. Yuan, E. Ng, A study on the impact of shadow-cast and tree species on in-canyon and neighborhood's thermal comfort, Building and Environment. 115 (2017) 1–17. https://doi.org/10.1016/j.buildenv.2017.01.005.

[19] T.E. Morakinyo, K.K.-L. Lau, C. Ren, E. Ng, Performance of Hong Kong's common trees species for outdoor temperature regulation, thermal comfort and energy saving, Building and Environment. 137 (2018) 157–170. https://doi.org/10.1016/j.buildenv.2018.04.012.

[20] N. Shin, A. Kotani, T. Sato, A. Sugimoto, T.C. Maximov, A. Nogovitcyn, Y. Miyamoto, H. Kobayashi, S. Tei, Direct measurement of leaf area index in a deciduous needle-leaf forest, eastern Siberia, Polar Science. 25 (2020) 100550. https://doi.org/10.1016/j.polar.2020.100550.

[21] Z. Liu, J.M. Chen, G. Jin, Y. Qi, Estimating seasonal variations of leaf area index using

litterfall collection and optical methods in four mixed evergreen–deciduous forests, Agricultural and Forest Meteorology. 209–210 (2015) 36–48. https://doi.org/10.1016/j.agrformet.2015.04.025.

[22] G. Yan, R. Hu, J. Luo, M. Weiss, H. Jiang, X. Mu, D. Xie, W. Zhang, Review of indirect optical measurements of leaf area index: Recent advances, challenges, and perspectives, Agricultural and Forest Meteorology. 265 (2019) 390–411. https://doi.org/10.1016/j.agrformet.2018.11.033.

[23] Beer, Bestimmung der Absorption des rothen Lichts in farbigen Flüssigkeiten, Annalen Der Physik. 162 (1852) 78–88. https://doi.org/10.1002/andp.18521620505.

[24] Y. Ryu, J. Verfaillie, C. Macfarlane, H. Kobayashi, O. Sonnentag, R. Vargas, S. Ma, D.D. Baldocchi, Continuous observation of tree leaf area index at ecosystem scale using upward-pointing digital cameras, Remote Sensing of Environment. 126 (2012) 116–125. https://doi.org/10.1016/j.rse.2012.08.027.

[25] W. Song, X. Mu, G. Yan, S. Huang, Extracting the Green Fractional Vegetation Cover from Digital Images Using a Shadow-Resistant Algorithm (SHAR-LABFVC), Remote Sensing. 7 (2015) 10425–10443. https://doi.org/10.3390/rs70810425.

[26] F. Chianucci, A. Cutini, Digital hemispherical photography for estimating forest canopy properties: current controversies and opportunities, IForest - Biogeosciences & Forestry. 5 (2012) 290–295. https://doi.org/10.3832/ifor0775-005.

[27] Z. Liu, C. Wang, J.M. Chen, X. Wang, G. Jin, Empirical models for tracing seasonal changes in leaf area index in deciduous broadleaf forests by digital hemispherical photography, Forest Ecology and Management. 351 (2015) 67–77. https://doi.org/10.1016/j.foreco.2015.05.005.

[28] Y. Li, Q. Guo, Y. Su, S. Tao, K. Zhao, G. Xu, Retrieving the gap fraction, element clumping index, and leaf area index of individual trees using single-scan data from a terrestrial laser scanner, ISPRS Journal of Photogrammetry and Remote Sensing. 130 (2017) 308–316. https://doi.org/10.1016/j.isprsjprs.2017.06.006.

[29] I. Indirabai, M.V.H. Nair, R.N. Jaishanker, R.R. Nidamanuri, Terrestrial laser scanner based 3D reconstruction of trees and retrieval of leaf area index in a forest environment, Ecological Informatics. 53 (2019) 100986. https://doi.org/10.1016/j.ecoinf.2019.100986.

[30] A. Peduzzi, R.H. Wynne, T.R. Fox, R.F. Nelson, V.A. Thomas, Estimating leaf area index in intensively managed pine plantations using airborne laser scanner data, Forest Ecology and Management. 270 (2012) 54–65. https://doi.org/10.1016/j.foreco.2011.12.048.

[31] D. Riaño, F. Valladares, S. Condés, E. Chuvieco, Estimation of leaf area index and covered ground from airborne laser scanner (Lidar) in two contrasting forests, Agricultural and Forest Meteorology. 124 (2004) 269–275. https://doi.org/10.1016/j.agrformet.2004.02.005.

[32] H. Tang, R. Dubayah, M. Brolly, S. Ganguly, G. Zhang, Large-scale retrieval of leaf area index and vertical foliage profile from the spaceborne waveform lidar (GLAS/ICESat), Remote Sensing of Environment. 154 (2014) 8–18. https://doi.org/10.1016/j.rse.2014.08.007.

[33] S. Luo, C. Wang, G. Li, X. Xi, Retrieving leaf area index using ICESat/GLAS full-waveform data, Remote Sensing Letters. 4 (2013) 745–753. https://doi.org/10.1080/2150704X.2013.790573.

[34] S.K. Behera, P. Srivastava, U.V. Pathre, R. Tuli, An indirect method of estimating leaf area index in Jatropha curcas L. using LAI-2000 Plant Canopy Analyzer, Agricultural and Forest Meteorology. 150 (2010) 307–311. https://doi.org/10.1016/j.agrformet.2009.11.009.

[35] N. Webb, C. Nichol, J. Wood, E. Potter, User Manual for the SunScan Canopy Analysis System type SS1 Version: 2.0, Delta-T Devices Ltd. Retrieved September. 11 (2013) 2019.
[36] S.G. Leblanc, J.M. Chen, M. Kwong, Tracing Radiation and Architecture of Canopies TRAC MANUAL Version 2.1, 2002. https://doi.org/10.4095/219952.
[37] LAI-2000 Plant Canopy Analyzer Operating Manual, Li-Cor, Inc, Lincoln, USA, 1992.
[38] R. Hu, E. Bournez, S. Cheng, H. Jiang, F. Nerry, T. Landes, M. Saudreau, P. Kastendeuch, G. Najjar, J. Colin, G. Yan, Estimating the leaf area of an individual tree in urban areas using terrestrial laser scanner and path length distribution model, ISPRS Journal of Photogrammetry and Remote Sensing. 144 (2018) 357–368. https://doi.org/10.1016/j.isprsjprs.2018.07.015.
[39] C. Macfarlane, M. Hoffman, D. Eamus, N. Kerp, S. Higginson, R. McMurtrie, M. Adams, Estimation of leaf area index in eucalypt forest using digital photography, Agricultural and Forest Meteorology. 143 (2007) 176–188. https://doi.org/10.1016/j.agrformet.2006.10.013.
[40] F. Chianucci, A. Cutini, P. Corona, N. Puletti, Estimation of leaf area index in understory deciduous trees using digital photography, Agricultural and Forest Meteorology. 198–199 (2014) 259–264. https://doi.org/10.1016/j.agrformet.2014.09.001.
[41] J. Liu, E. Pattey, Retrieval of leaf area index from top-of-canopy digital photography over agricultural crops, Agricultural and Forest Meteorology. 150 (2010) 1485–1490. https://doi.org/10.1016/j.agrformet.2010.08.002.
[42] Y. Wang, Z. Ni, S. Chen, B. Xia, Microclimate regulation and energy saving potential from different urban green infrastructures in a subtropical city, Journal of Cleaner Production. 226 (2019) 913–927. https://doi.org/10.1016/j.jclepro.2019.04.114.
[43] Y. Li, Y. Song, Optimization of Vegetation Arrangement to Improve Microclimate and Thermal Comfort in an Urban Park, International Review for Spatial Planning and Sustainable Development. 7 (2019) 18–30. https://doi.org/10.14246/irspsd.7.1_18.
[44] T.E. Morakinyo, K.K.-L. Lau, C. Ren, E. Ng, Performance of Hong Kong's common trees species for outdoor temperature regulation, thermal comfort and energy saving, Building and Environment. 137 (2018) 157–170. https://doi.org/10.1016/j.buildenv.2018.04.012.
[45] F. Chianucci, N. Puletti, E. Giacomello, A. Cutini, P. Corona, Estimation of leaf area index in isolated trees with digital photography and its application to urban forestry, Urban Forestry & Urban Greening. 14 (2015) 377–382. https://doi.org/10.1016/j.ufug.2015.04.001.
[46] S. Wei, T. Yin, M.A. Dissegna, A.J. Whittle, G.L.F. Ow, M.L.Mohd. Yusof, N. Lauret, J.-P. Gastellu-Etchegorry, An assessment study of three indirect methods for estimating leaf area density and leaf area index of individual trees, Agricultural and Forest Meteorology. 292–293 (2020) 108101. https://doi.org/10.1016/j.agrformet.2020.108101.
[47] T.A. Black, J.-M. Chen, X. Lee, R.M. Sagar, Characteristics of shortwave and longwave irradiances under a Douglas-fir forest stand, Canadian Journal of Forest Research. (2011). https://doi.org/10.1139/x91-140.
[48] F. Chianucci, A note on estimating canopy cover from digital cover and hemispherical photography, Silva Fennica. 50 (2015). https://doi.org/10.14214/sf.1518.
[49] J. Pisek, Y. Ryu, K. Alikas, Estimating leaf inclination and G-function from leveled digital camera photography in broadleaf canopies, Trees. 25 (2011) 919–924. https://doi.org/10.1007/s00468-011-0566-6.
[50] Y. Ryu, T. Nilson, H. Kobayashi, O. Sonnentag, B.E. Law, D.D. Baldocchi, On the correct estimation of effective leaf area index: Does it reveal information on clumping effects?,

Agricultural and Forest Meteorology. 150 (2010) 463–472. https://doi.org/10.1016/j.agrformet.2010.01.009.

[51] Z. Jie, P. Zhong, W. Hou, Y. Zuo, P. Leng, Estimating Needle and Shoot Inclination Angle Distributions and Projection Functions in Five Larix principis-rupprechtii Plots via Leveled Digital Camera Photography, Forests. 12 (2020) 30. https://doi.org/10.3390/f12010030.

[52] Y. Ryu, O. Sonnentag, T. Nilson, R. Vargas, H. Kobayashi, R. Wenk, D.D. Baldocchi, How to quantify tree leaf area index in an open savanna ecosystem: A multi-instrument and multi-model approach, Agricultural and Forest Meteorology. 150 (2010) 63–76. https://doi.org/10.1016/j.agrformet.2009.08.007.

[53] X. Zou, M. Mõttus, P. Tammeorg, C.L. Torres, T. Takala, J. Pisek, P. Mäkelä, F.L. Stoddard, P. Pellikka, Photographic measurement of leaf angles in field crops, Agricultural and Forest Meteorology. 184 (2014) 137–146. https://doi.org/10.1016/j.agrformet.2013.09.010.

[54] J. Pisek, O. Sonnentag, A.D. Richardson, M. Mõttus, Is the spherical leaf inclination angle distribution a valid assumption for temperate and boreal broadleaf tree species?, Agricultural and Forest Meteorology. 169 (2013) 186–194. https://doi.org/10.1016/j.agrformet.2012.10.011.

[55] Z. Zhu, C. Kleinn, N. Nölke, Assessing tree crown volume—a review, Forestry: An International Journal of Forest Research. 94 (2021) 18–35. https://doi.org/10.1093/forestry/cpaa037.

[56] W.-M. Wang, Z.-L. Li, H.-B. Su, Comparison of leaf angle distribution functions: Effects on extinction coefficient and fraction of sunlit foliage, Agricultural and Forest Meteorology. 143 (2007) 106–122. https://doi.org/10.1016/j.agrformet.2006.12.003.

[57] A.R.G. Lang, X. Yueqin, Estimation of leaf area index from transmission of direct sunlight in discontinuous canopies, Agricultural and Forest Meteorology. 37 (1986) 229–243. https://doi.org/10.1016/0168-1923(86)90033-X.

[58] F. Chen, Z. Zhou, P. Wang, H. Li, Y. Zhong, Green space vegetation quantity in workshop area of Wuhan Iron and Steel Company, Ying Yong Sheng Tai Xue Bao. 17 (2006) 592–596.

[59] Xueyan Guo, Research on the living vegetation volume of common landscape plants in Nanjing, Thesis, Nanjing Forestry University, 2009.

[60] C. Wang, Z.-H. Wang, Y.-H. Ryu, A single-layer urban canopy model with transmissive radiation exchange between trees and street canyons, Building and Environment. 191 (2021) 107593. https://doi.org/10.1016/j.buildenv.2021.107593.

[61] Y.-H. Ryu, E. Bou-Zeid, Z.-H. Wang, J.A. Smith, Realistic Representation of Trees in an Urban Canopy Model, Boundary-Layer Meteorol. 159 (2016) 193–220. https://doi.org/10.1007/s10546-015-0120-y.

[62] Z.-H. Wang, Monte Carlo simulations of radiative heat exchange in a street canyon with trees, Solar Energy. 110 (2014) 704–713. https://doi.org/10.1016/j.solener.2014.10.012.

[63] Z. Li, X. Feng, J. Sun, C. Li, W. Yu, Z. Fang, STMRT: A simple tree canopy radiative transfer model for outdoor mean radiant temperature, Building and Environment. 228 (2023) 109846. https://doi.org/10.1016/j.buildenv.2022.109846.

[64] B.N. Bailey, M. Overby, P. Willemsen, E.R. Pardyjak, W.F. Mahaffee, R. Stoll, A scalable plant-resolving radiative transfer model based on optimized GPU ray tracing, Agricultural and Forest Meteorology. 198–199 (2014) 192–208. https://doi.org/10.1016/j.agrformet.2014.08.012.

[65] E.S. Krayenhoff, T. Jiang, A. Christen, A. Martilli, T.R. Oke, B.N. Bailey, N. Nazarian, J.A. Voogt, M.G. Giometto, A. Stastny, B.R. Crawford, A multi-layer urban canopy meteorological model with trees (BEP-Tree): Street tree impacts on pedestrian-level climate, Urban Climate. 32 (2020) 100590. https://doi.org/10.1016/j.uclim.2020.100590.

[66] X. Li, A.H. Strahler, Modeling the gap probability of a discontinuous vegetation canopy, IEEE Trans. Geosci. Remote Sensing. 26 (1988) 161–170. https://doi.org/10.1109/36.3017.